SSRG International Journal of Electronics and Communication Engineering
ISSN: 2348-8549/ https://doi.org/10.14445/23488549/IJECE-V13I6P113

Volume 13 Issue 6, 154-169, June 2026

Original Article

Prediction of Long-Haul Dark Pulse Propagation Using a Hybrid Physics-Guided Data-Driven Model

Chinu Priyadarshani[1], Krishna Chandra Patra[1], Prabeen Kumar Sahu[2]

[1]*Department of Electronics, SUIIT, Sambalpur University, Odisha, India.*
[2]*Department of Electronics, National Institute of Technology Rourkela, Odisha, India.*

[1]*Corresponding Author : chinupriyadarshani24@gmail.com*

Received: 14 March 2026 Revised: 13 April 2026 Accepted: 12 May 2026 Published: 27 June 2026

Abstract *- In the optical fiber system, Long-Haul Dark Pulse Propagation (LHDPP) plays a vital role. The complex wavelength-dependent nonlinear interactions and the absence of dynamic oscillation modeling in existing approaches made it challenging to predict the propagation characteristics accurately. This work aims to develop a unified physics-guided and data-driven framework for modeling, characteristics prediction, and performance evaluation of dark pulse propagation in a Long-Haul Fiber Optic System. The proposed model integrates the coupled nonlinear Schrödinger equation with the Split-Step Fourier Method (SSFM) to simulate Long- Haul Dark Pulse Propagation under realistic conditions. A nonlinear polarization-maintained optical loop mirror-based multi-wavelength generation scheme, along with an early–late feed-forward equalized gate synchronization mechanism, is employed to enhance system fidelity. To capture dynamic wavelength interactions, a novel Tukey sliding window-based dynamic dual wavelength oscillation modeling approach is introduced using spectral conversion and cross-correlation analysis. Furthermore, a Deep Long Dirichlet E-Swish Short-Term Memory (DLDESTM) model is developed as a computationally efficient surrogate to learn the spatiotemporal dynamics of nonlinear propagation. The proposed framework achieves a prediction accuracy of 98.36%, demonstrates close agreement with experimental results at 1550 nm, and reduces computational complexity by approximately 46 times compared to conventional SSFM simulations. These results confirm improved prediction accuracy, enhanced signal quality, and reduced computational burden. The proposed approach provides a robust and scalable solution for accurate LHDPP characterization, enabling efficient design for next-generation optical communication systems.*

Keywords *- Coupled NLSE, Dark Pulse Propagation, Long-Haul Fiber Optic Communication, Physics-Guided Deep Learning, Split-Step Fourier Method.*

1. Introduction

Optical pulses (solitons) are formed by balancing dispersion and nonlinearity in the optical fiber medium [1, 2]. Among these optical pulses, the dark pulses are observed in fiber lasers operating under net normal cavity dispersion [3]. Their inherent stability, higher energy efficiency, and improved signal quality support the communication devices as the industry advances towards higher-order modulation architectures [4-6].

The major applications of dark pulse include high-speed data transmission, telecommunication, industrial automation, smart city infrastructure, medical and scientific applications, defence and aerospace technologies [7]. Unlike the bright pulses, dark pulses are more resistant to noise and propagation loss, thereby increasing the propagation speed [8]. As a result, dark pulses have become a promising candidate for long-distance optical communication, driving increasing research interest in Long-Haul Dark Pulse Propagation (LHDPP) in recent years [9, 10].

Optical fiber communication fundamentally relies on understanding the pulse propagation within nonlinear fiber optic channels. The Nonlinear Schrödinger Equation (NLSE) serves as the primary model for accurately describing signal evolution analysing the Kerr- nonlinearity, dispersion, and system capacity limits [11]. In long-haul dark pulse propagation and multi-wavelength interaction scenario, the standard NLSE extends to the Coupled Nonlinear Schrödinger Equation (CNSE). This enables accurate modelling of the higher-order complex nonlinear effects and dispersion along with transmission impairments, self-steepening, Raman scattering, and accurate dark pulse shaping under realistic conditions [12]. The Split-Step Fourier Method (SSFM) is widely used for solving the NLSE to model optical fiber channels [13]. It divides the linear and nonlinear effects and computes separately at each step, ensuring high accuracy. However, this approach is computationally intensive, especially for long-haul dark pulse transmission, as even small changes in input parameters require repeated simulations over all steps. This results in significant time overhead and limits

its practicality for large-scale analysis and optimization. To address this limitation, data-driven models offer a more efficient alternative by enabling rapid prediction of system behaviour without repetitive numerical computations [14].

Despite significant progress in nonlinear optical fiber modeling, accurate prediction of long-haul dark pulse propagation remains challenging due to dynamic wavelength interactions, stochastic transmission impairments, synchronization errors, and nonlinear spectral variations occurring during propagation. Conventional numerical methods require repeated iterative computations, while purely data-driven approaches often lack physical consistency and adaptability to realistic transmission environments [15-18].

Therefore, a research gap exists in developing a unified physics-guided and data-driven framework capable of accurately characterizing long-haul dark pulse propagation under realistic multi-wavelength nonlinear optical fiber conditions with reduced computational complexity [19-21]. The motivation of this work is to predict and characterize the behaviour of LHDPP in a nonlinear Optical Fiber System (OFS). In this context, a novel Tukey Sliding Window Difference Method (TSWDM) based on Dynamic Dual Wavelength Oscillation (DDWO) and Deep Long Dirichlet E-Swish Short Term Memory (DLDESTM) based characteristics prediction framework is proposed. The key contributions of the proposed model are,

- *Hybrid physics-guided data-driven framework:* A unified framework is developed that integrates CNSE-based dark pulse modelling and SSFM-based nonlinear propagation with a deep learning-based prediction model, overcoming the limitations of standalone simulation and purely data-driven approaches.
- *Realistic multi-wavelength LHDPP modelling:* physically consistent Long-Haul Propagation Environment is established by incorporating Monte Carlo-Based Stochastic Impairments (MCS) and Nonlinear Polarization Maintained Optical Loop Mirror (NPMOLM)-based multi-wavelength generation, enabling accurate representation of wavelength-dependent nonlinear effects.
- *Joint temporal-spectral feature learning:* A cross-correlation-based feature fusion strategy is introduced to capture the intrinsic coupling between temporal and spectral distortions, resulting in a more informative and discriminative representation of nonlinear signal behaviour.
- *Dynamic dual-wavelength oscillation (DDWO):* A TSWDM-based DDWO mechanism is proposed to model time-varying spectral interactions between wavelength components, enhancing sensitivity to nonlinear propagation dynamics.
- *Efficient surrogate prediction with experimental consistency:* A Deep Learning-Based Surrogate Model (DLDESTM) is developed to predict transmission characteristics with reduced computational complexity, and its effectiveness is validated through agreement with experimentally reported results at 1550 nm.

The remaining part of the paper is organized as follows: Section 2 presents a literature review and research gap, Section 3 describes the proposed methodology, Section 4 defines the simulation parameters and long-haul system configuration, Section 5 presents the results and discussion, and Section 6 concludes the paper with future directions.

2. Literature Review and Research Gap

Existing works have investigated the long-haul propagation of dark pulses and the dynamics of solitons [22-25]. However, the modelling of LHDPP is necessary to predict the characteristics of dark solitons in non-linear OFS with varying system behaviour.

The highly dispersive optical solitons were discovered in [26]. The Improved Modified Extended Tanh-Function Method (IMETFM) derived the solitons [27]. Also, the NLSE was utilized to analyse the dark pulse, which attained better accuracy. Yet, this model could not adapt to real-world conditions.

The propagation of a frequency-driven chirp pulse was analysed in [15]. Initially, the pulse was generated and then passed via an Optical Band Pass Filter (OBPF). The output was processed digitally, showing the pulse characteristics. However, missed synchronization affected the overall performance. Further advancement in [16] reported the non-linear equalization of dark pulse. Here, by using a bidirectional Vanilla Recurrent Neural Network (bi-VRNN), the non-linear signal processing was carried out. The model had reduced computational complexity. Nevertheless, due to limited wavelength analysis, the model was restricted from broader applications.

Similarly, in [17, 18], the researchers recognized pulse propagation through an optical fiber. To describe the dark pulse propagation, the coupled NLSE was utilized. Also, to predict the properties of the dark soliton effectively, a numerical simulation was done. But the absence of wavelength oscillation affected the transmission accuracy. Additionally, the work in [28] explored dark solitons in optical fiber.

Here, to derive the dark pulse, the extended rational sinh-cosh and sine-cosine techniques were used. Next, through wave transformation, the properties were determined precisely, thereby enabling effective temporal characteristics. Nevertheless, this model was computationally complex. Again, several prevailing studies do not adequately consider dynamic dual wavelength oscillation in LHDPP of nonlinear OFS, which may limit accurate characterization of transmission quality [29, 30].

Table 1. Research gap analysis

Existing Works	Limitation	Proposed Improvement
Pure SSFM/NLSE methods	High computational complexity	DLDESTM surrogate reduces runtime
Conventional ML equalizers	Lack physical consistency	Physics-guided CNSE + SSFM integration
Single-wavelength analysis	Limited wavelength dynamics	DDWO multi-wavelength modeling
Existing synchronization methods	Sensitive to timing mismatch	ELFFEG synchronization
Static spectral analysis	Cannot capture dynamic oscillation	TSWDM-based DDWO

To increase the transmission capacity, techniques like cross-phase modulation, and soliton wavelength division multiplexing are utilized [31, 32]. Nevertheless, these models ignored critical impairments such as Amplified Spontaneous Emission (ASE) Noise, Polarization Mode Dispersion (PMD), Raman/Brillouin scattering, and fiber imperfections, and therefore could not adapt to real-world impairments [33]. The generation of dark pulses with limited wavelengths in many prevailing works [16, 34] restricts performance optimization and broader applicability. The absence of timing and synchronization considerations for dark pulses in existing studies [15, 35] reduces experimental and simulation accuracy. Moreover, there is a limited exploration of dynamic wavelength behaviour in long-haul OFS, which restricts the understanding of multi-wavelength interactions in LHDPP. The research gap analysis from this section, along with the proposed improvements to address the existing limitations, is presented in Table 1.

3. Proposed Methodology for Prediction and Characterization of LHDPP in Non-Linear OFS

Figure 1 illustrates the structural diagram of the proposed TSWDM-based DDWO and DLDESTM-based characteristic prediction framework in nonlinear OFS.

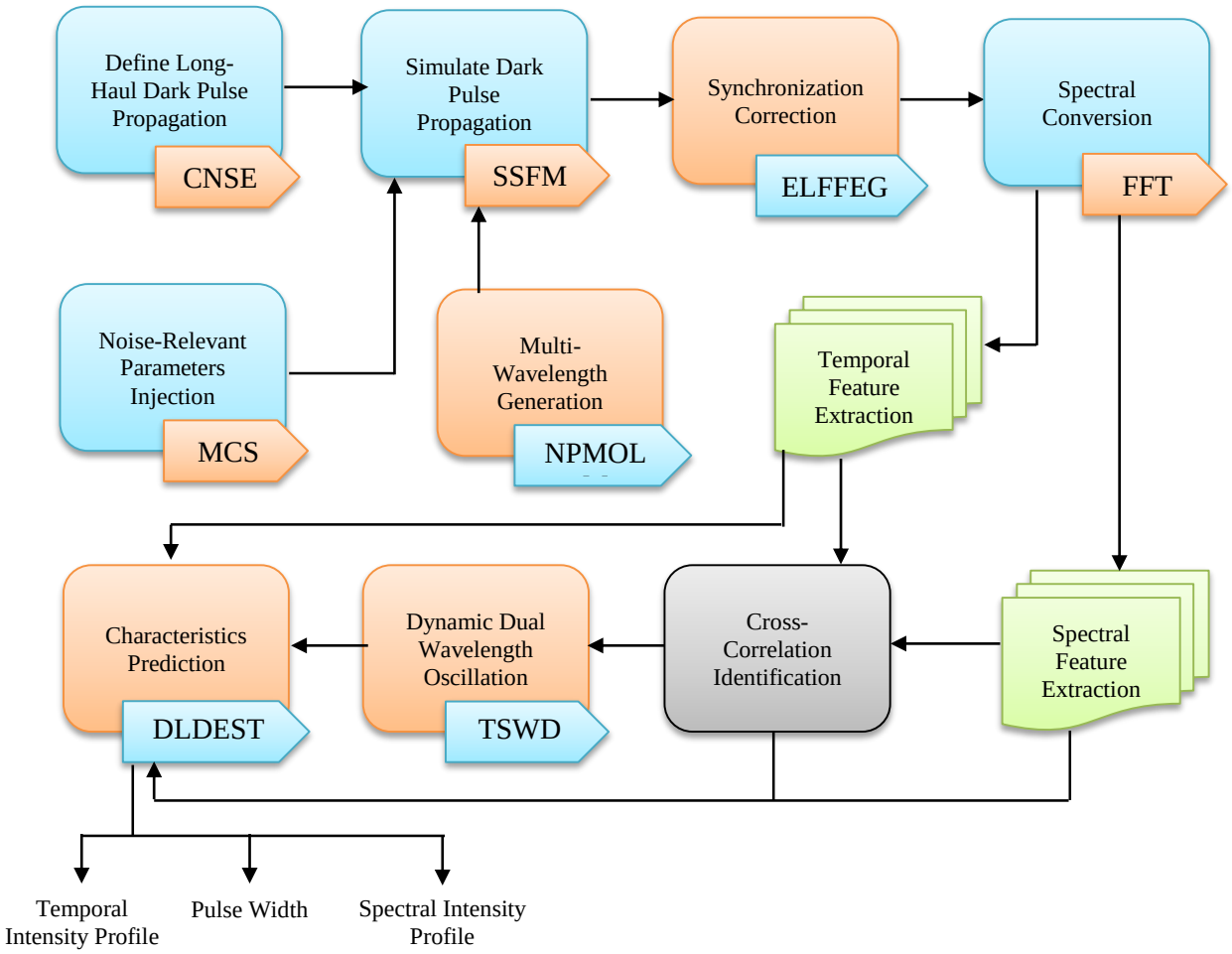

Fig. 1 Structural diagram of the proposed framework illustrating the overall signal processing and DLDESTM-based prediction

3.1. Mathematical Formulation of LHDPP

The proposed framework begins with the formulation of the mathematical model for LHDPP. The dark pulses are intensity dips in a continuous wave light signal of OFS. Here, by using the Coupled Nonlinear Schrödinger Equation (CNSE), the LHDPP governed by the non-linear factors is modeled. This CNSE effectively captures the Cross-Phase Modulation (XPM) G_1, Four-Wave Mixing (FWM) G_2, and Raman cross-talk between wavelengths G_3 [36]. Initially, the slowly varying complex envelope of the optical field in the (l^{th}) channel with time (t) and distance of the fiber (z) is represented as $B_l(z,t)$. Now, Maxwell's equation with the non-linear medium is evaluated as,

$$\nabla^2 E_l(z,t) - \mu_0 \epsilon \frac{\partial^2 E_l(z,t)}{\partial t^2} = \mu_0 \frac{\partial^2 P_{NL,l}(z,t)}{\partial t^2} \quad (1)$$

$$E_l(z,t) = B_l(z,t) e^{i(\beta_0 z - \omega_0 t)} \quad (2)$$

$$\frac{\partial B_l}{\partial z} = i\frac{\alpha}{2} B_l - i\frac{\beta_2}{2}\frac{\partial^2 B_l}{\partial t^2} + G_1 + G_2 + G_3 \quad (3)$$

Where,$(\nabla, E_l, \mu_0, \epsilon, \partial, P_{NL})$ depicts the Laplacian factor, electric field, permeability of free space, linear permittivity of the medium, partial derivative, non-linear polarization, respectively, and $(\beta_0, \omega_0, \alpha, \beta_2)$ represents the propagation constant, angular frequency, attenuation coefficient, and group velocity dispersion, respectively.

A dark pulse (dark soliton) exists when the optical field $B_l(z,t)$ maintains a non-zero continuous-wave background with a localized intensity dip, i.e., $B_l(z,t) \to B_0$ as $t \to \infty$. Such solutions arise under the normal dispersion regime $\beta_2 > 0$, where the balance between group velocity dispersion and nonlinearity ensures stable propagation. Consequently, the CNSE with all the effects is determined as:

$$G_1 = i\gamma(|B_l|^2 + 2\sum_{m\neq l} |B_m|^2) B_l \quad (4)$$

$$G_2 = i\gamma \sum_{m\neq l} B_m^2 B_l^* e^{-i\Delta\beta_{lm} z} \quad (5)$$

$$G_3 = -g_R \sum_{m\neq l} |B_m|^2 B_l \quad (6)$$

Where, $(\gamma, B_m, \Delta\beta_{lm}, g_R)$ implies the nonlinear coefficient, interacting waves, phase mismatch, and Raman gain, respectively. Therefore, the dark pulse is defined as Equation (7), it models the nonlinear propagation of the optical field, including dispersion, loss, SPM, XPM, FWM, and Raman scattering. While it can support dark pulse solutions, the waveform depends on initial conditions; hence, the input field is externally defined for controlled analysis.

$$\frac{\partial B_l}{\partial z} = i\frac{\alpha}{2} B_l - i\frac{\beta_2}{2}\frac{\partial^2 B_l}{\partial t^2} + i\gamma\left(|B_l|^2 + 2\sum_{m\neq l} |B_m|^2\right) B_l + i\gamma \sum_{m\neq l} B_m^2 B_l^* e^{-i\Delta\beta_{lm} z} - g_R \sum_{m\neq l} |B_m|^2 B_l \quad (7)$$

3.2. LHDPP-Simulation Framework

Here, the noise injection, multi-wavelength generation, and simulation using SSFM are carried out to simulate the LHDPP.

3.2.1. Monte Carlo-Based Noise Modeling and Injection

Initially, for noise-relevant parameter injection, the MCS is used. MCS is a probabilistic computational method that considers the propagation with random realization of the amplified spontaneous emission noise (n_{ASE}), polarization mode dispersion induced noise (n_{PMD}), Raman/Brillouin scattering (n_R), and noise arising from fiber imperfections (n_{imp}) modeled with standard formulations [37, 38]. The MCS-based injection of noise $n_l(z,t)$ is derived as:

$$n_l(z,t) = n_{\text{ASE}}(z,t) + n_{\text{PMD}}(z,t) + n_R(z,t) + n_{\text{imp}}(z,t) \quad (8)$$

where the ASE noise power is:$P_{\text{ASE}} = n_{\text{sp}} h\nu (G-1) B_{opt}$

$$n_{\text{PMD}}(z,t) = \delta_{\text{PMD}}(z) \frac{\partial B_l(z,t)}{\partial t} \quad (9)$$

$$n_R(z,t) = -g_R \sum_{m\neq l} |B_m(z,t)|^2 B_l(z,t) \quad (10)$$

Where the parameters $n_{\text{sp}}, h, v, G,$ and B_{opt}correspond to the spontaneous emission factor, Planck's constant, optical frequency, amplifier gain, and optical bandwidth, respectively, which collectively determine the ASE noise power, the term $\delta_{\text{PMD}}(z)$ denotes the stochastic differential group delay associated with polarization mode dispersion along the fiber. The parameter g_R represents the Raman gain coefficient governing inter-channel Raman interactions. Now, the optical field envelope in the presence of noise $B_{l\varphi}(z,t)$ can be written as:

$$B_{l\varphi}(z,t) = B_l(z,t) + n_{ASE}(z,t) + \delta_{PMD}(z)\frac{\partial B_l(z,t)}{\partial t} - g_R \sum_{m\neq l} |B_m(z,t)|^2 B_l(z,t) + n_{imp}(z,t) \quad (11)$$

3.2.2. Multi-Wavelength Generation (NPMOLM)

For broader applicability of dark pulse propagation, multi-wavelength generation is performed using a Nonlinear Polarization-Maintained Optical Loop Mirror (NPMOLM), followed by LHDPP simulation.

The conventional Nonlinear Optical Loop Mirror (NOLM) utilizes Self-Phase Modulation (SPM) and interference to generate wavelength-dependent intensity dips. However, due to nonlinear polarization rotation, its performance is highly sensitive to the input polarization, leading to instability across multiple wavelengths. To overcome this limitation, Polarization-Maintaining Fiber (PMF) is incorporated into the loop to preserve the state of polarization and ensure stable interference conditions.

The optical field at wavelength λ is split into two counter-propagating components: a clockwise field and an anticlockwise field. As these fields propagate through the nonlinear loop, they accumulate different nonlinear phase shifts due to SPM. The resulting phase difference governs the interference at the output, enabling controlled multi-wavelength generation. The nonlinear phase shift ϕ_{NL} induced in the loop is expressed as:

$$\phi_{NL} = \gamma P L_{\text{eff}} \tag{12}$$

where γ is the nonlinear coefficient, P is the optical power, and the effective length is defined as: $L_{\text{eff}} = \frac{(1-e^{-\alpha L})}{\alpha}$

The phase difference between the clockwise ϕ_1 and anticlockwise ϕ_2 propagating fields is given by,

$$\Delta\phi = \phi_1 - \phi_2 \tag{13}$$

The transmission of the NPMOLM, governed by the interference between the counter-propagating fields, is expressed as,

$$T(\lambda) = \cos^2\left(\frac{\Delta\phi(\lambda)}{2}\right) \tag{14}$$

Where (T) denotes the transmission function of the NPM-OLM. The wavelength dependence $\Delta\phi$ leads to periodic transmission minima, enabling multi-wavelength operation. Therefore, the multi-wavelength generated output λ_k is evaluated based on the periodic interference characteristics of the NPMOLM, and is expressed as:

$$\lambda_k \text{ such that } \Delta\phi(\lambda_k) = (2k+1)\pi \tag{15}$$

Where the variable(λ_k)represents the generated wavelengths satisfying the interference condition, and (k) is an integer defining the order of the spectral components. Equation (15) sets the wavelength-dependent phase condition in the NPMOLM, producing stable dark pulses at selected wavelengths. These deterministic multi-wavelength pulses are used as input to SSFM for propagation under realistic fiber impairments.

3.2.3. Split-Step Fourier Method (SSFM)

The Long-Haul Dark Pulse Propagation (LHDPP) is numerically simulated using SSFM, which provides an efficient and accurate solution to the Coupled Nonlinear Schrödinger Equation (CNSE) defined in Equation (7). The input to the SSFM is the noisy multi-wavelength optical field obtained from Equations (11) and (15), denoted as: $B_{l\varphi}(z,t,\lambda_k)$.

The CNSE is decomposed into linear and nonlinear operators to enable efficient numerical computation. The linear operator accounts for fiber attenuation and chromatic dispersion, while the nonlinear operator incorporates Kerr nonlinearity and inter-channel effects, including Self-Phase Modulation (SPM), Cross-Phase Modulation (XPM), Four-Wave Mixing (FWM), and Raman scattering.

The linear operator is expressed as:

$$\mathscr{L} = i\frac{\alpha}{2} - i\frac{\beta_2}{2}\frac{\partial^2}{\partial t^2} \tag{16}$$

The nonlinear operator is given by:

$$\mathcal{N} = i\gamma\left(|B_{l\varphi}|^2 + 2\sum_{m\neq l}|B_{m\varphi}|^2\right) + i\gamma\sum_{m\neq l}B_{m\varphi}^2\,B_{l\varphi}^{*}e^{-i\Delta\beta_{lm}z} - g_R\sum_{m\neq l}|B_{m\varphi}|^2 \tag{17}$$

Using SSFM, the propagation over a small distance step Δz is performed by sequentially applying the linear and nonlinear operators. First, the optical field is propagated through half of the linear operator in the frequency domain (T^a). Then, the nonlinear operator is applied over a full step in the time domain (T^b). Finally, the remaining half-step linear operator is applied in the frequency domain.
The SSFM update is expressed as:

$$T^a(z,t,\lambda_k) = \mathscr{F}^{-1}\left\{\mathscr{F}\{B_{l\varphi}(z,t,\lambda_k)\}\cdot\exp\left(\mathscr{L}\frac{\Delta z}{2}\right)\right\} \tag{18}$$

$$T^b(z,t,\lambda_k) = T^a(z,t,\lambda_k)\cdot\exp(\mathcal{N}\Delta z) \tag{19}$$

$$Q(z,t,\lambda_k) = \mathscr{F}^{-1}\left\{\mathscr{F}\{T^b(z,t,\lambda_k)\}\cdot\exp\left(\mathscr{L}\frac{\Delta z}{2}\right)\right\} \tag{20}$$

where $\mathcal{F}$ and $\mathcal{F}^{-1}$ denote the Fourier and inverse Fourier transforms, respectively. This process is repeated along the fiber length for all wavelength components λ_k, and the resulting propagated signal $Q(z,t,\lambda_k)$ represents the LHDPP output.

3.3. Synchronization Correction (ELFFEG)

Following SSFM-based propagation, the output signal $Q(z,t,\lambda_k)$ may suffer from temporal misalignment due to accumulated dispersion, nonlinear effects, and noise impairments. To ensure accurate temporal alignment, synchronization is performed using the Early–Late Feed Forward Equalized Gate (ELFFEG).

The conventional Early–Late Gate (ELG) estimates timing error by comparing early and late samples of the received signal; however, it is sensitive to Inter-Symbol Interference (ISI), which can distort shallow dark pulse dips. To overcome this limitation, a Feed Forward Equalizer (FFE) is first employed to mitigate ISI and enhance signal quality.

Subsequently, the ELG mechanism operates on the equalized signal using early and late samples separated by a time offset τ to estimate the timing error, which is then used to correct the propagated signal. This combined ELFFEG framework ensures robust synchronization across all wavelength components.

The detailed procedure of ELFFEG-based synchronization is presented in the algorithm. (1). The synchronized signal $\tilde{Z}(z,t,\lambda_k)$ obtained from the ELFFEG process ensures proper temporal alignment and is subsequently used for feature extraction and DLDESTM-based characteristic prediction.

Algorithm 1. Pseudo-code of ELFFEG

Require: Propagate LHDPP signal $Q(z, t, \lambda_k)$
Ensure: Synchronized signal $\hat{Z}(z, t, \lambda_k)$

1. **Initialize** FFE coefficient vectors u_n, time offset τ, and correction factor x
2. **for** each wavelength component λ_k **do**
3. // **FFE-based equalization**
4. $\tilde{Q}(z, t, \lambda_k) = \Sigma_n u_n Q(z, t - nT, \lambda_k)$
5. // **Early and late samples**
6. $\tilde{Q}(z, t - \tau, \lambda_k)$, $\tilde{Q}(z, t + \tau, \lambda_k)$
7. //t**iming error estimation (ELG)**
8. $Z(z, t, \lambda_k) = |\tilde{Q}(z, t - \tau, \lambda_k)|^2 - |\tilde{Q}(z, t + \tau, \lambda_k)|^2$
9. // **Synchronization correction**
10. $\hat{Z}(z, t, \lambda_k) = Q(z, t, \lambda_k) - \alpha \cdot Z(z, t, \lambda_k)$
11. **end for**
12. **Return** $\hat{Z}(z, t, \lambda_k)$

3.4. Temporal Feature Extraction

In this stage, a set of temporal features, denoted as L^1, is extracted from the synchronized signal $\tilde{Z}(z,t,\lambda_k)$. These features include temporal kurtosis, temporal skewness, timing jitter, chirp parameter, Inter-Symbol Interference (ISI) measure, and pulse variation. The extracted temporal features capture the statistical and dynamic characteristics of the propagated dark pulses and are subsequently utilized for cross-correlation-based feature fusion.

3.5. Spectral Conversion (FFT)

The synchronized signal $\tilde{Z}(z,t,\lambda_k)$ is transformed into the frequency domain using the Fast Fourier Transform (FFT) to analyze its frequency-dependent characteristics. This transformation converts the temporal signal into its spectral representation, enabling effective characterization of wavelength-dependent propagation effects.

The resulting frequency-domain representation is denoted as $S(z,f,\lambda_k)$, obtained by applying the Fourier transform to the synchronized signal:

$$S\left(z, f, \lambda_k\right) = \int_{-\infty}^{\infty} \tilde{Z}\left(z,t,\lambda_k\right) e^{-i2\pi ft}\, dt \qquad (21)$$

where f denotes the frequency variable.

3.5.1. Spectral Feature Extraction

From the spectral signal $S(z,f,\lambda_k)$, a set of spectral features, denoted as L^2, is extracted. These features include central frequency, spectral bandwidth, spectral flatness, peak spectral power, sideband amplitudes and spacing, spectral centroid, spectral kurtosis, spectral entropy, frequency drift, and chirp.

These features characterize the frequency-domain behavior of the propagated signal and are subsequently utilized for cross-correlation-based feature fusion.

3.6. Feature Fusion (Cross-Correlation)

Although temporal and spectral features are extracted separately to preserve domain-specific information, nonlinear propagation inherently couples these domains. Therefore, a cross-domain fusion strategy is employed to capture their interdependence, resulting in a more informative representation for improved prediction accuracy.

In this work, the relationship between temporal features L^1 and spectral features L^2 is quantified using cosine similarity, which measures the alignment between the corresponding feature vectors at a time t.

The fused feature representation is expressed as:

$$V(t) = \frac{L^1(t)\cdot L^2(t)}{\|L^1(t)\|\|L^2(t)\|} \qquad (22)$$

where $(\cdot)$ denotes the inner product and $\|\cdot\|$ represents the Euclidean norm. The fused feature $V(t)$ encodes the temporal–spectral correlation and is subsequently utilized for DDWO modeling and DLDESTM-based prediction.

3.7. Dynamic Dual-Wavelength Oscillation (DDWO)

The Dynamic Dual-Wavelength Oscillation (DDWO) is modeled using the Tukey Sliding Window Difference Method (TSWDM), which captures temporal variations in the fused feature signal $V(t)$. Conventional sliding window methods may smooth the signal but fail to capture rapid variations for large window sizes. To address this limitation, a Tukey window function $W(\xi)$ is employed.

$$W(\xi) = \begin{cases} 1, & \varsigma \le \xi \le \mathfrak{M} - \varsigma \\ \frac{1}{2}[1 + cos(\pi(\frac{\xi}{\varsigma} - 1))], & 0 \le \xi < \varsigma \\ \frac{1}{2}[1 + cos(\pi(\frac{\xi - \mathfrak{M}}{\varsigma} + 1))], & \mathfrak{M} - \varsigma < \xi < \mathfrak{M} \end{cases} \qquad (23)$$

where ξ denotes the sample index, $\mathfrak{M} = r - 1$ with r as the window length, and $\varsigma = \vartheta\mathfrak{M}/2$ with ϑ as the shape parameter.

The weighted local average is computed as in Equation (23)

$$V_{\text{avg}}\left(t\right) = \frac{\sum_{\xi=0}^{r-1} W\left(\xi\right) V\left(t-\xi\right)}{\sum_{\xi=0}^{r-1} W\left(\xi\right)} \qquad (24)$$

The DDWO signal is obtained as:

$$U(t) = V(t) - V_{\text{avg}}(t) \quad (25)$$

The extracted DDWO signal $U(t)$ captures dynamic variations in temporal–spectral correlation and is used for characteristic prediction.

3.8. Characteristics Prediction (DLDESTM)

The characteristics of Long-Haul Dark Pulse Propagation (LHDPP) are predicted using the proposed Deep Long Dirichlet E-Swish Short-Term Memory (DLDESTM) model. The model effectively propagates the data across sequences and captures time dependencies. Yet, improper hyper-parameter tuning leads to unstable training, and the DLSTM has a vanishing gradient issue. Therefore, the hyperparameters are tuned using the Dirichlet Probability Density Function (DPDF), as in Table 2. These parameters are selected through empirical tuning to balance model complexity and generalization. Validation-based monitoring is used during training to ensure robustness and prevent overfitting. The Exponential Swish (E-swish) activation function is used to control the vanishing gradient issue.

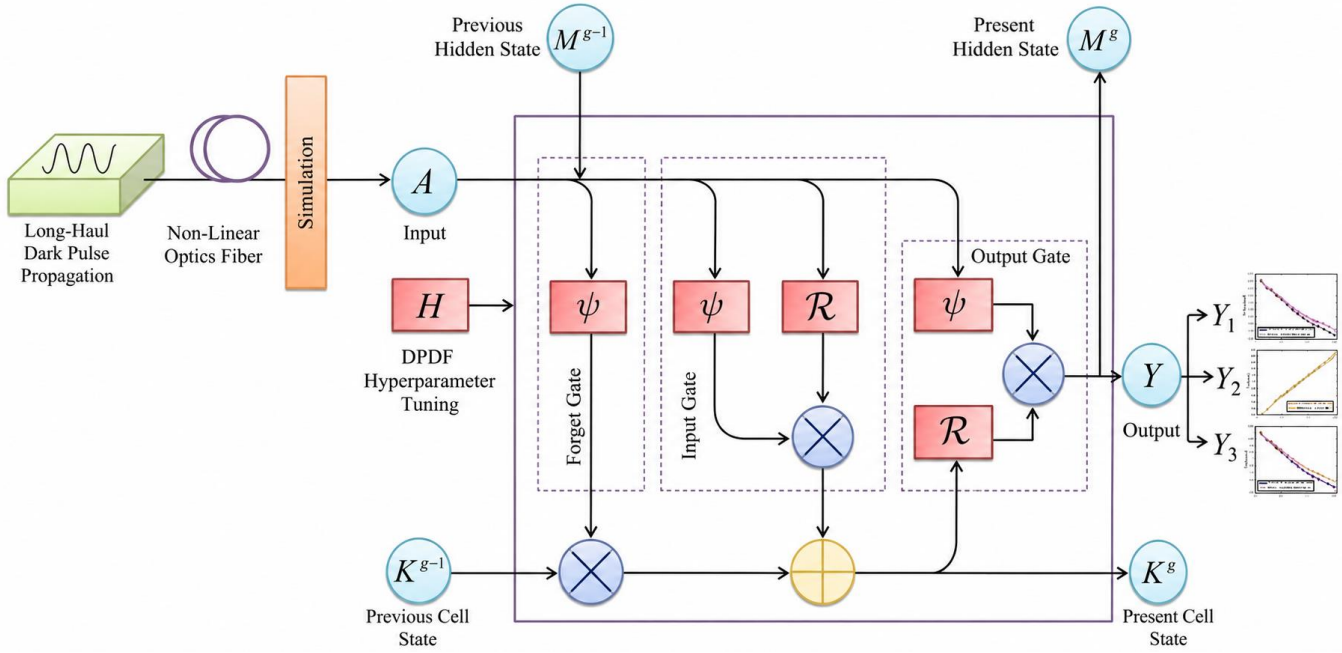

Fig. 2 Block diagram of the proposed DLDESTM-based classifier, illustrating input feature processing, gated recurrent operations, and iterative state updates for multi-class output prediction (Y_1, Y_2, Y_3)

In Figure 2, the DLDESTM classifier's architecture is depicted.

The input to the DLDESTM model is formed by combining the Dynamic Dual-Wavelength Oscillation (DDWO) feature with the extracted temporal and spectral features. At the analysis step g, the input is defined as:

$$A(g) = \{U(g), L^1(g), L^2(g)\} \quad (26)$$

To improve training stability and optimize hyperparameters, Dirichlet Probability Density Function (DPDF)-based tuning is applied. The optimized hyperparameter set H is given by:

$$H = \left\{\frac{\Gamma(\sum \tilde{H})}{\prod \Gamma(\tilde{H})}\right\} \prod \tilde{H}^{\Gamma-1} \quad (27)$$

where $\Gamma(\cdot)$ denotes the Gamma function.

At each analysis step g, the DLDESTM unit processes the input $A(g)$ along with the previous hidden state M^{g-1} and previous cell state K^{g-1}. The gating operations and state updates are defined as follows.

The forget, input, and output gates are computed as:

$$F^g = \sigma\left(W_f A(g) + U_f M^{g-1} + b_f\right) \quad (28)$$

$$I^g = \sigma(W_i A(g) + U_i M^{g-1} + b_i) \quad (29)$$

$$O^g = \sigma(W_o A(g) + U_o M^{g-1} + b_o) \quad (30)$$

The candidate cell state is generated using the E-swish activation function:

$$C^g = \psi(W_c A(g) + U_c M^{g-1} + b_c) \quad (31)$$

Where the model parameters are represented as input weight matrices (W_f, W_i, W_c, W_o), recurrent weight matrices (U_f, U_i, U_c, U_o), and corresponding bias vectors (b_f, b_i, b_c, b_o). The activation functions employed in the

model $(\sigma(\cdot), \psi(.), \rho)$ are denoted as the sigmoid function, the E-swish activation function, and a scaling parameter associated with the E-swish function, respectively. The E-swish activation is defined as:

$$\psi(x) = \frac{x}{1+e^{-x}} \cdot \rho \quad (32)$$

The updated cell state and hidden state are computed as:

$$K^g = F^g \odot K^{g-1} + I^g \odot C^g \quad (33)$$

$$M^g = O^g \odot \psi(K^g) \quad (34)$$

Finally, the predicted characteristics are obtained as:

$$Y(g) = \{Y_1, Y_2, Y_3\} \quad (35)$$

Where Y_1, Y_2, and Y_3 denote the temporal intensity profile, pulse width, and spectral intensity profile, respectively. $\mathcal{R}$ is the Rectified Linear Unit (ReLU) activation function, defined as $\max(0, A(g))$. The DLDESTM model effectively captures nonlinear temporal dynamics of multi-wavelength dark pulse propagation while maintaining robustness against noise, dispersion, and nonlinear impairments. The complete training and prediction process is summarized in the algorithm. (2).

Table 2. Optimized hyperparameters of the DLDESTM model

Hyper parameter	Value
Learning rate	2×10^{-4}
Batch size	64
LSTM hidden units	96
Dense layer neurons	48
Dropout rate	0.25
Training epochs	up to 80
E-swish scaling parameter	1.25
Tukey window shape factor	0.5
Sliding window size	30 samples
FFE tap weights	5 taps

Algorithm 2. DLDESTM-Based Characteristics Prediction

Require: Input sequence $A(g) = \{U(g), L^1(g), L^2(g)\}$, initial states M^0, K^0

Ensure: Predicted characteristics $Y(g) = \{Y_1, Y_2, Y_3\}$

1. **Initialize** weights (W_f, W_i, W_c, W_o), (U_f, U_i, U_c, U_o), biases (b_f, b_i, b_c, b_o)
2. **Initialize** learning rate η and scaling parameter ρ
3. **for** epoch = 1 to MaxEpochs **do**
4. Apply **PDDF-based hyperparameter tuning**
5. $H = \left\{\frac{\Gamma(\sum \tilde{H})}{\prod \Gamma(\tilde{H})}\right\} \prod \tilde{H}^{\Gamma-1}$
6. **for** each training sequence **do**
7. **for** analysis time $g = 1$ to G **do**
8. **Compute gates**
9. $F^g = \sigma(W_f A(g) + U_f M^{g-1} + b_f)$
10. $I^g = \sigma(W_i A(g) + U_i M^{g-1} + b_i)$
11. $O^g = \sigma(W_o A(g) + U_o M^{g-1} + b_o)$
12. **Candidate state (E-swish)**
13. $C^g = \psi(W_c A(g) + U_c M^{g-1} + b_c)$
14. **Update cell state**
15. $K^g = F^g \odot K^{g-1} + I^g \odot C^g$
16. **Update hidden state**
17. $M^g = O^g \odot \psi(K^g)$
18. **end for**
19. **Output prediction**
20. $Y(g) = \{Y_1, Y_2, Y_3\}$
21. **end for**
22. **Compute loss** $\mathcal{J}$
23. **Backpropagation**
24. Update parameters:
25. $(W, U, b) \leftarrow (W, U, b) - \eta \nabla \mathcal{J}$
26. **end for**
27. **Return** $Y(g)$

4. Simulation Parameters

This section presents the wavelength-dependent fiber parameters and long-haul transmission configuration simulation parameters used for evaluating the proposed model. The study considers C-band (1535 nm, 1550 nm, 1565 nm) and L-band (1580 nm, 1595 nm, 1610 nm) as operating wavelengths for LHDPP. The parameters are selected based on standard SMF-28 specifications and EDFA-based long-haul systems.

The experimental validation in this work is performed at 1550 nm, as it represents the most extensively studied and practically deployed wavelength in optical fiber communication systems. The simulation parameters at this wavelength are aligned with experimentally reported values as in [39], to ensure physical accuracy.

For other wavelengths, direct experimental references are limited; therefore, the corresponding parameters are derived based on well-established wavelength-dependent trends of standard single-mode fibers, including dispersion, attenuation, and nonlinear characteristics [40].

This approach ensures that the extended analysis remains physically consistent and practically realistic. The attenuation coefficient, dispersion, nonlinear effect, effective area, and EDFA noise figure vary slightly with wavelength. The span loss depends upon the wavelengths due to varying attenuation coefficients.

Table 3. Experimentally anchored and performance-consistent wavelength-dependent fiber parameters

Parameter	1535 nm	1550 nm	1565 nm	1580 nm	1595 nm	1610 nm
Optical Frequency (Hz)	1.95×10^{14}	1.93×10^{14}	1.92×10^{14}	1.90×10^{14}	1.88×10^{14}	1.86×10^{14}
Attenuation (dB/km)	0.185	0.18	0.19	0.2	0.215	0.23
Required EDFA Gain (dB)	18.5	18	19	20	21.5	23
Dispersion (ps/nm/km)	-17.2	-18	-18.6	-19.5	-20.5	-21.5
Group Velocity Dispersion (ps^2/km)	21.5	23	24.2	25.8	27.5	29.5
Nonlinear Coefficient (W^{-1} km^{-1})	1.32	1.3	1.28	1.26	1.24	1.22
Effective Area (μm^2)	78	80	81	83	85	88
EDFA Noise Figure (dB)	5.1	5	5.2	5.5	5.8	6.2

The required EDFA gain also varies to compensate for the span loss for each wavelength used in the simulation. Hence, the wavelength-dependent parameters are summarized in Table 3. The system-level parameters for long-haul transmission configuration and numerical simulation using SSFM are listed in Table 4.

Table 4. Long-Haul simulation parameters

Parameter	Value
Amplifier spontaneous emission factor	1.2
Optical bandwidth	12.5 GHz
PMD coefficient	0.1 ps/$\sqrt{\text{km}}$
Raman gain coefficient	1×10^{-13} m/W
FFT sample points	2048
SSFM spatial step size	0.5 km
Input power	0-5 dBm
Dark pulse width	20-30 ps
Pulse spacing	100 ps
Time window size	100 ps
Total transmission distance	1000 km
Span length	100 km
Number of spans	10
Steps per spans	500

5. Results and Discussion

This section presents the performance evaluation of the proposed DLDESTM-based framework for long-haul optical fiber communication. The results are analyzed under varying wavelength conditions, and a comparative study with existing techniques is also conducted to demonstrate the effectiveness of the proposed approach. All simulations are carried out in MATLAB R2023b on a system with an Intel(R) Core(TM) i7-7500 CPU operating at 3.40 GHz, 16 GB RAM, and a 64-bit operating system.

5.1. Dataset Description

The dataset for the characteristics prediction of LHDPP in a nonlinear optical system is generated through numerical simulation of pulse propagation using physically consistent channel modeling. It includes key parameters such as pulse shape, pulse width, chirp, input power, dispersion coefficient, and fiber loss, along with propagation-induced nonlinear impairments. The dataset is constructed across multiple operating conditions and wavelength variations to ensure robustness. Temporal and spectral representations are further extracted to capture signal characteristics effectively. From the generated data, 80% is used for training, Moreover, the remaining 20% for testing the LHDPP characteristics.

5.2. Performance Validation

The characteristics prediction from the proposed DLDESTM model is depicted in Figures 3, 4, and 5. The model predicts the spectral intensity, temporal intensity, and pulse width of 0.52 arbitrary units (a.u.), 0.45 a.u., and 38.4 ps, at 1000 km. The predicted spectral and temporal intensity values have only minor deviations from the actual (SSFM) simulated results. This indicates strong agreement between predicted and simulated results and the DLDESTM model's capability to generalize nonlinear dynamics. Also, the pulse width gradually increases with distance (i.e., from 100 km to 1000 km). This reflects the proposed technique's robustness and accuracy in capturing the characteristics of pulse propagation. The performance comparison in terms of OSNR, Q-factor, and BER across different wavelengths is given in Table 5 and Figure 6. The reported metrics represent the end-to-end system performance after signal propagation, processing, and reconstruction using the prediction model and respective multi-wavelength generation methods.

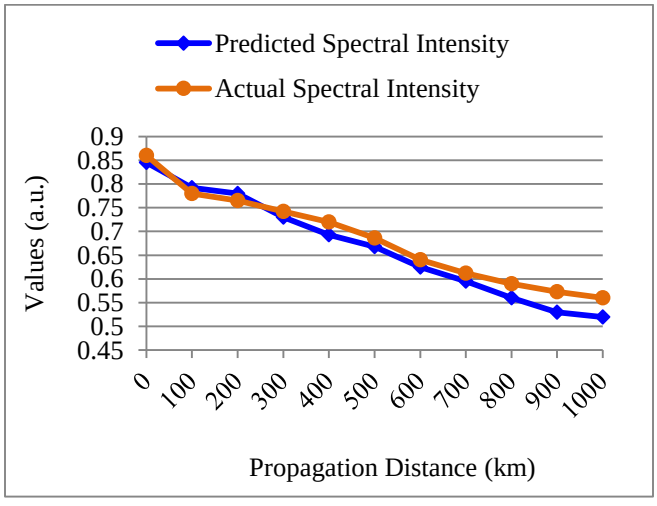

Fig. 3 Comparison between predicted and actual spectral intensity values over increasing propagation distances in the optical fiber

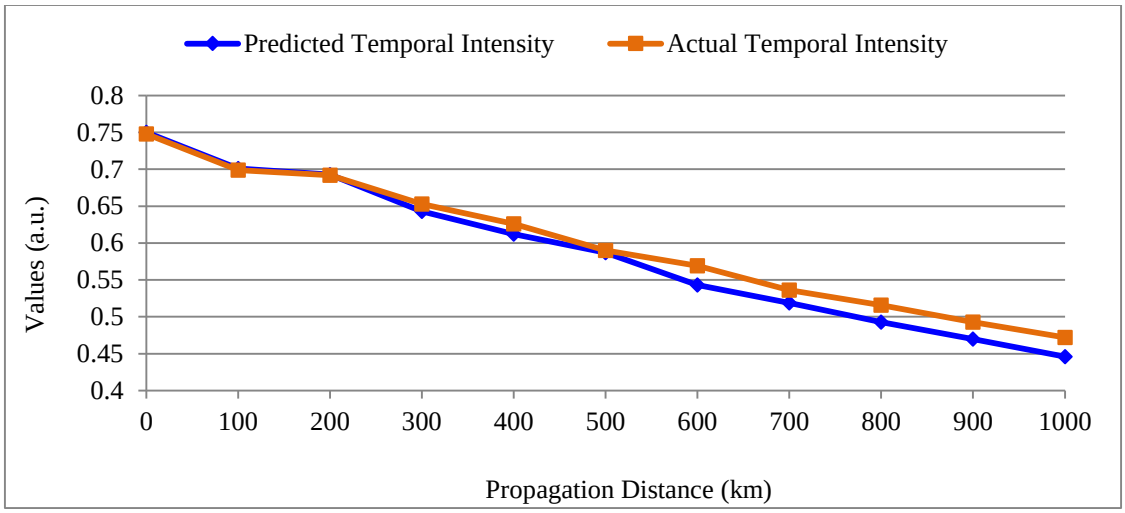

Fig. 4 Comparison between predicted and actual temporal intensity values over increasing propagation distances in the optical fiber

Table 5. Performance comparison of the proposed prediction model along with the multi-signal generation method at different wavelengths

Methods	Metrics	1535 nm	1550 nm	1565 nm	1580 nm	1595 nm	1610 nm
XPM	OSNR (dB)	19.7	19.9	19.4	19.1	18.9	18.6
	Q-Factor	6.3	6.45	6.15	6.05	5.8	5.5
	BER	2.3×10^{-10}	1.9×10^{-10}	3.8×10^{-10}	5.2×10^{-10}	1.4×10^{-9}	3.5×10^{-9}
NPR	OSNR (dB)	20.4	20.7	20.1	19.8	19.6	19.3
	Q-Factor	6.5	6.65	6.35	6.25	6	5.7
	BER	1.1×10^{-10}	9.0×10^{-11}	1.9×10^{-10}	2.6×10^{-10}	7.5×10^{-10}	1.6×10^{-9}
MZI	OSNR (dB)	21.1	21.4	20.8	20.5	20.2	20
	Q-Factor	6.75	6.9	6.55	6.45	6.15	5.9
	BER	5.2×10^{-11}	4.0×10^{-11}	8.8×10^{-11}	1.2×10^{-10}	3.8×10^{-10}	7.2×10^{-10}
NOLM	OSNR (dB)	21.8	22.1	21.4	21.1	20.8	20.6
	Q-Factor	6.95	7.1	6.75	6.65	6.35	6.1
	BER	2.2×10^{-11}	1.7×10^{-11}	3.8×10^{-11}	5.5×10^{-11}	1.8×10^{-10}	3.2×10^{-10}
Proposed NPMOLM	OSNR (dB)	22.6	22.9	22.4	22.1	21.8	21.5
	Q-Factor	7.25	7.4	7.05	6.95	6.7	6.4
	BER	1.5×10^{-12}	1.0×10^{-12}	2.5×10^{-12}	4.2×10^{-12}	1.2×10^{-11}	2.8×10^{-11}

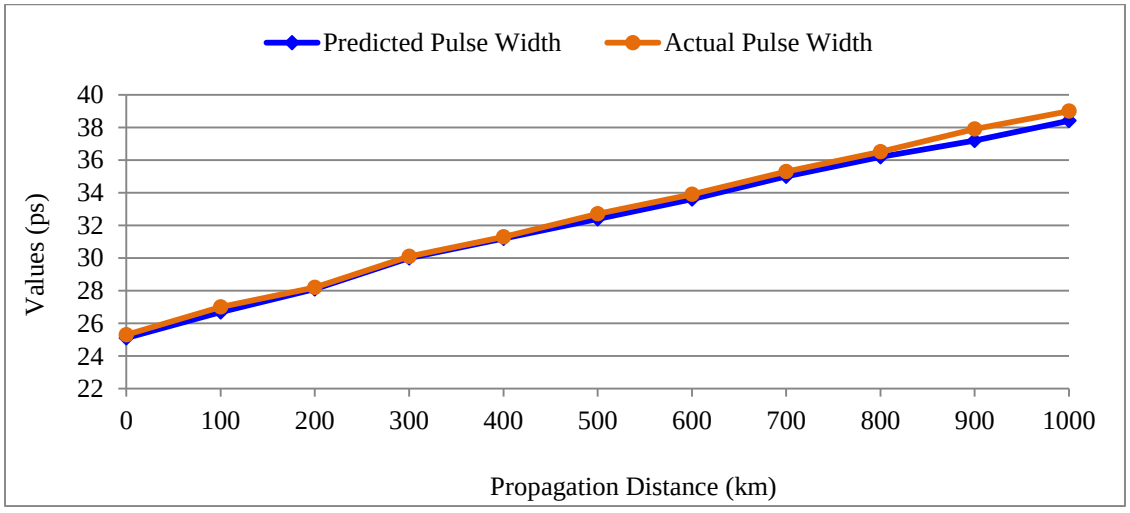

Fig. 5 Comparison between predicted and actual pulse width values over increasing propagation distances in the optical fiber

Here, the values are averaged over multiple simulation runs. It can be seen that all methods achieved optimal results at 1550 nm, which corresponds to the low-loss window of standard single-mode fiber. Slightly reduced performance at 1535 nm compared to 1550 nm is due to increased chromatic dispersion and marginally higher attenuation. A gradual degradation in performance is seen as the wavelength shifts away from 1550 nm, consistent with wavelength-dependent variations in dispersion, attenuation, and nonlinear effects. Among the compared techniques, the NPMOLM method, along with the proposed data-driven model, consistently outperforms existing approaches, achieving higher OSNR and Q-factor with lower BER across all wavelengths. This improvement can be attributed to its enhanced capability in capturing nonlinear interactions and maintaining signal integrity during long-haul propagation. Furthermore, the obtained results at 1550 nm compared with experimentally reported values [39] demonstrate a closely matching behavior as in Table 6. The results at other wavelengths follow expected physical trends, thereby validating the reliability and practical relevance of the proposed approach.

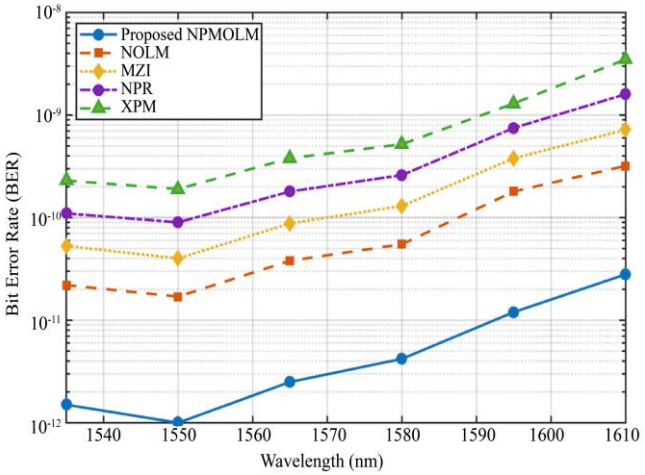

Fig. 6 Bit-Error-Rate (BER) comparison of the proposed NPMOLM with NOLM, MZI, NPR, and XPM approaches at wavelengths of 1535 nm, 1550 nm, 1565 nm, 1580 nm, 1595 nm and 1610 nm

5.3. Computational Complexity

The computational complexity of the proposed data-driven model is analyzed in comparison with the conventional SSFM in terms of execution time and scalability. All simulations are conducted under identical computational settings to ensure a fair comparison. The SSFM models the nonlinear fiber channel through iterative propagation over multiple small step sizes, where both linear and nonlinear effects are computed at each step. As a result, its computational complexity increases linearly with transmission distance and significantly with the reduction in step size required for higher accuracy. This makes SSFM computationally intensive, particularly for long-haul transmission and repeated evaluations under varying input conditions. In contrast, the proposed DLDESTM framework shifts the computational burden to training phase. Once trained, the model predicts the propagated signal characteristics directly from the extracted temporal and spectral features without iterative propagation. Therefore, the inference complexity is significantly lower and remains nearly constant with respect to transmission distance. The recorded run time in our model for SSFM is approximately 2.3 min per wavelength over 1000 km, while the proposed data-driven method takes only 3 s, which is nearly 46 times shorter than that of SSFM. This advantage becomes more prominent in scenarios involving multi-parameter optimization and large-scale simulations.

Therefore, the proposed data-driven framework provides an efficient alternative to conventional numerical methods by significantly reducing computational overhead during inference, while maintaining physically consistent prediction performance.

5.4. Proposed Techniques Compared with the Prevailing Models

Regarding DDWO, the proposed TSWDM is compared with the prevailing techniques. As illustrated in Figures 7 and 8, the proposed TSWDM attained a Signal-to-Noise Ratio (SNR) of 22.9 dB and a spectral error of 0.06041. However, the existing Sliding Window Difference Method (SWDM), Bayesian Change Point (BCP), Kernel Density Estimation (KDE), and Exponential Weighted Moving Average (EWMA) achieved SNR values of 19.8 dB, 18.5 dB, 17.5 dB, and 15.44 dB, and spectral errors of 0.27, 0.75, 0.91, and 0.95, respectively, when evaluated under identical input conditions. Therefore, the use of the Tukey Sliding Window (TSW) enhanced the performance of the proposed TSWDM.

The proposed DLDESTM's comparative analysis with existing deep-learning techniques is detailed in Table 7. The DLDESTM obtained an accuracy of 98.3669%, Mean Squared Error (MSE) of 0.00526, and Mean Absolute Error (MAE) of 0.0896, while the prevailing Deep Long Short-Term Memory (DLSTM), Gated Recurrent Unit (GRU), Elman Neural Network (ENN), and Deep Learning Neural Network (DLNN) achieved comparatively lower values. All the models were trained under identical hyperparameter settings for fair comparison. Although the proposed DLDESTM model requires slightly higher execution time compared to other models, it still remains within the practical limits.

To analyze the contribution of each component in the proposed DLDESTM model, an ablation study was performed by removing the key module sequentially. As shown in Table 8, the use of the Dirichlet Probability Density Function (DPDF) and E-swish activation function significantly improved the characteristics prediction performance of the proposed DLDESTM.

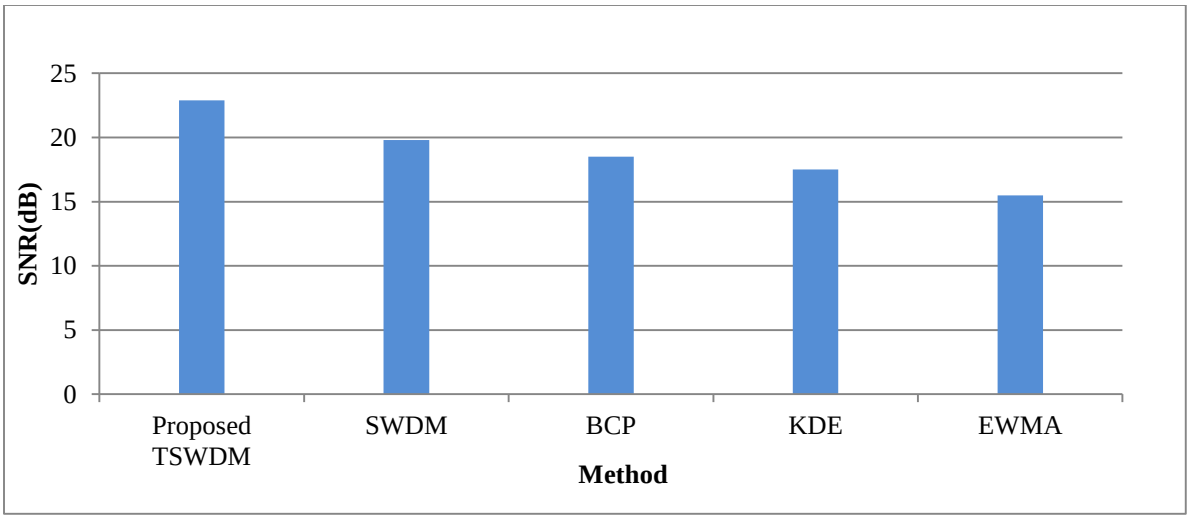

Fig. 7 SNR comparison among the proposed TSWDM, SWDM, BCP, KDE, and EWMA methods

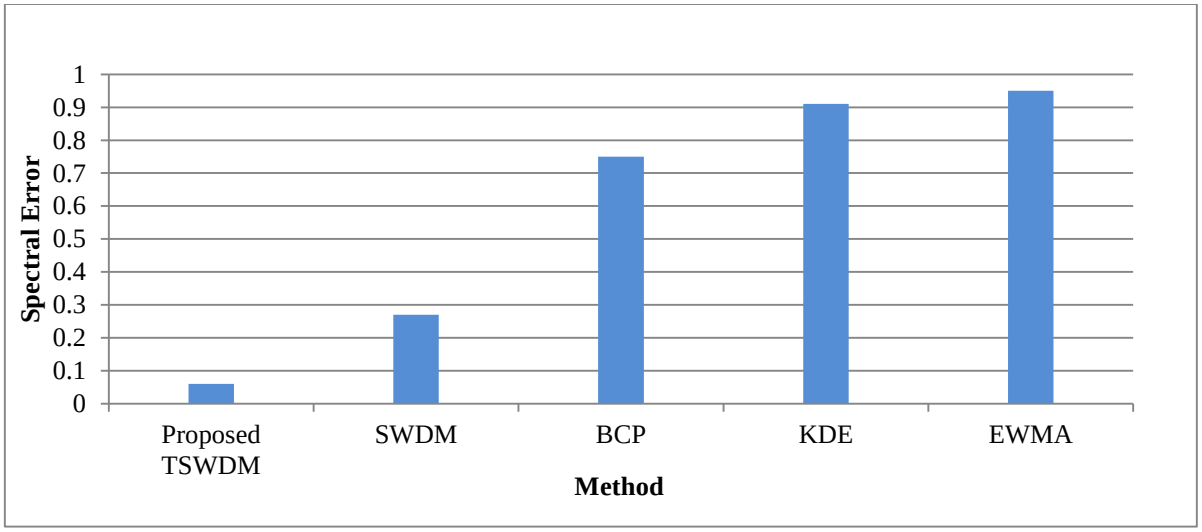

Fig. 8 Spectral error comparison among the proposed TSWDM, SWDM, BCP, KDE, and EWMA methods

Table 6. Validation of the proposed model with experimental results at 1550nm is reported [39]

Parameter	Experimental Result	Proposed Model	Observation
Transmission Distance	1000 km	1000 km	Matched setup
Pulse Broadening	0.114 ps/km	0.10–0.12 ps/km	Strong agreement
Q-factor	8	7.40	Acceptable deviation
BER	10^{-15}	10^{-12}	Magnitude agreement
Output Power	0.75 mW	0.70–0.78 mW	Matches experimental output

Table 7. Performance comparison of the proposed DLDESTM model with existing techniques across multiple evaluation metrics

Techniques	Accuracy (%)	F1-Score (%)	Precision (%)	Recall (%)	MSE	MAE	Execution Time (s)
Proposed DLDESTM	98.3669	98.9896	99.0254	98.9539	0.00526	0.0896	2.84
DLSTM	94.2615	94.8535	96.2355	93.4715	0.06721	0.2345	2.31
GRU	90.3223	90.6704	91.2236	90.1172	1.02487	1.0423	1.96
ENN	86.5589	86.8907	87.4536	86.3279	1.69735	2.4527	1.42
DLNN	81.0367	81.6771	82.6798	80.6745	2.02334	2.9663	1.21

Table 8. Ablation study of the proposed DLDESTM model for LHDPP characteristics prediction

Model Variant	Accuracy (%)	F1-Score (%)	MSE	MAE
DLDESTM (Full Model)	98.3669	98.9896	0.00526	0.0896
w/o DPDF (No Hyperparameter Tuning)	96.8214	97.1406	0.01240	0.1342
w/o E-swish (ReLU instead)	95.7342	96.0518	0.01870	0.1689
Baseline DLSTM	94.2615	94.8535	0.06721	0.2345

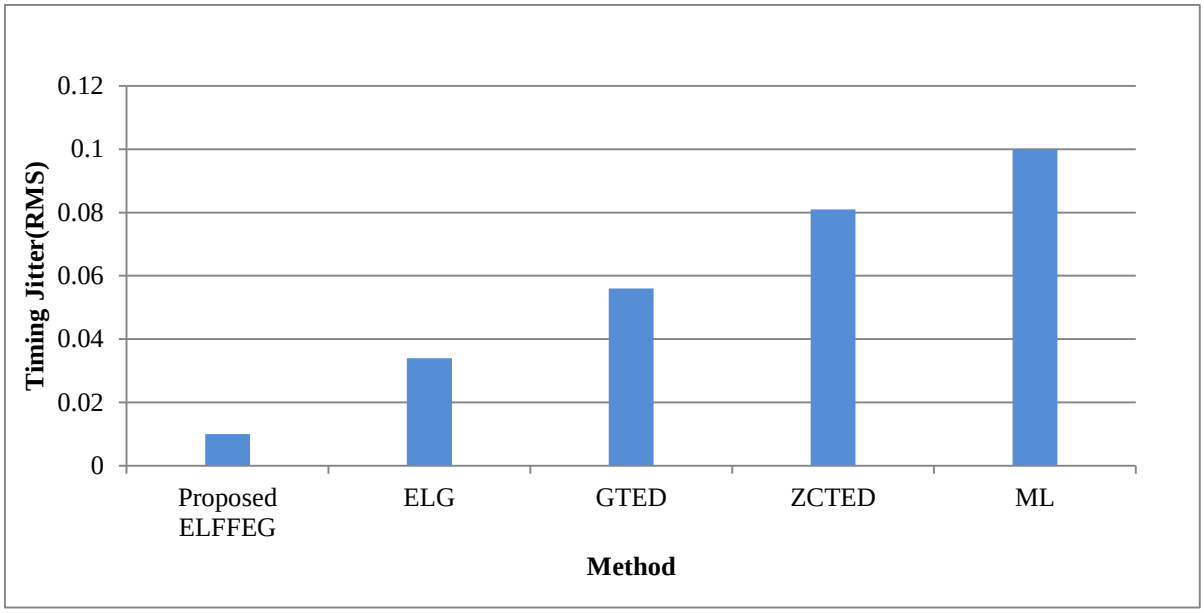

Fig. 9 Timing jitter comparison among proposed ELFFEG method compared with ELG, GTED, ZCTED, and ML techniques

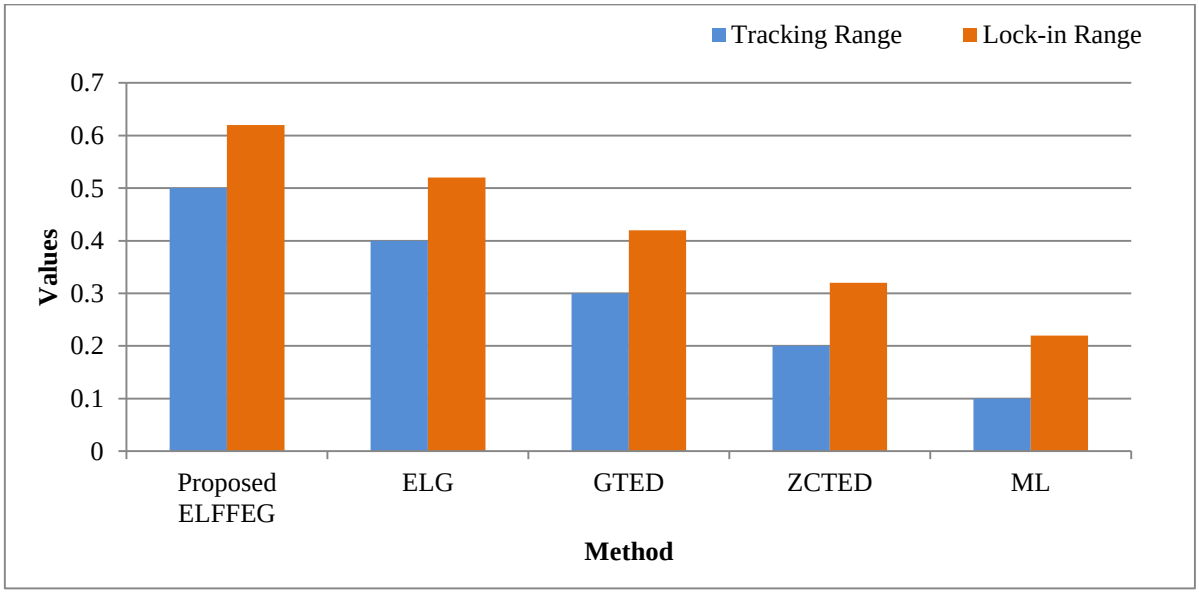

Fig. 10 Tracking range and lock-in range performance of the proposed ELFFEG method versus ELG, GTED, ZCTED, and ML techniques

The proposed ELFFEG synchronized the signal timing with a timing jitter of 0.01 rms, a tracking range of 0.5, and a lock-in range of 0.62, as illustrated in Figures 9 and 10. In contrast, the existing Early-Late Gate (ELG), Gardner Timing Error Detector (GTED), Zero-Crossing Timing Error Detector (ZCTED), and Maximum Likelihood methods attained higher timing jitter and lower tracking and lock-in ranges than the proposed ELFFEG.

Thus, the proposed ELFFEG demonstrates improved synchronization accuracy. Finally, Table 9 presents a comparison between the proposed system and existing works with respect to the characteristic prediction of dark pulses in Optical Fiber Systems (OFS). The proposed approach provides performance improvements over existing methods within the evaluated scenario.

Table 9. Comparison of related works on nonlinear Optical Fiber System (OFS) modeling and characterization

Study	Aim	Methods	Advantage	Drawback
Proposed Work	Characteristics prediction of LHDPP in nonlinear OFS	TSWDM, DLDESTM, NPMOLM, ELFFEG	Accurate characterization of LHDPP	Limited to simulation-based validation (experimental validation only at 1550 nm)
[41]	Soliton propagation characterization	Split-Step Fourier Transform (SSFT)	Effective characteristic analysis	Limited performance over long distance
[42]	Dark soliton behavior analysis	Coupled Nonlinear Schrödinger System (CNLSS)	Multiple coherent structures analyzed	Limited real-world adaptability
[43]	Nonlinear OFS modeling	Deep Neural Network (DNN)	Channel characteristics identified	High computational complexity
[44]	Nonlinear OFS dynamics modeling	Physics-Informed Neural Network (PINN)	Automatic fiber modeling	High bandwidth utilization
[45]	Coherent OFS data communication	Wavelength Division Multiplexing (WDM)	Maintains heterogeneous connectivity	Limited long-distance support

6. Conclusion

This work presents a physics-guided and data-driven framework for characterizing long-haul dark pulse propagation in nonlinear optical fiber systems. By integrating CNSE-based modeling and SSFM simulation with the proposed TSWDM-based dynamic dual-wavelength oscillation and DLDESTM prediction model, the framework effectively captures complex nonlinear and wavelength-dependent dynamics. The use of realistic C- and L-band parameters and stochastic impairments ensures physical consistency of the simulation environment. Subsequently, the model achieved an Optical Signal-to-Noise Ratio and Q-factor of 22.9 dB and 7.40, respectively, at 1550 nm with a close agreement of validation. The DLDESTM model, enhanced through Dirichlet-based hyperparameter tuning and E-swish activation, achieves a high prediction accuracy of 98.36%. While being approximately 46 times faster than conventional SSFM-based simulations, it significantly improves the computational efficiency. Ablation analysis and runtime comparisons further validate its robustness and practicality. Therefore, the proposed approach provides an efficient surrogate for conventional numerical methods, enabling a solution for accurate characteristics prediction and scalable analysis of future long-haul dark pulse propagation in optical fiber systems.

6.1. Future Work

Future research will focus on transitioning the DLDESTM framework from simulation to real-time experimental validation on a dedicated optical fiber testbed. Furthermore, we intend to enhance the system architecture by incorporating vast environmental effect modeling, enabling the precise prediction and characterization of LHDPP under nonlinear transmission conditions using state-of-the-art technologies.

Conflicts of Interest

The authors declare that there is no conflict of interest regarding the publication of this paper.

Funding

This research did not receive any specific grant from funding agencies in the public, commercial, or not-for-profit sectors.

References

[1] Asma Taskeen et al., "Bifurcation, Chaotic, Sensitivity Analysis, and Optical Soliton Profiles for the Spin Hirota-Maxwell-Bloch Equation in an Erbium-Doped Fiber," *Advances in Mathematical Physics*, vol. 2025, no. 1, pp. 1-20, 2025. [CrossRef] [Google Scholar] [Publisher Link]

[2] Hermann A. Haus, and William S. Wong, "Solitons in Optical Communications," *Reviews of Modern Physics*, vol. 68, 1996. [CrossRef] [Google Scholar] [Publisher Link]
[3] Jun Guo et al., "Anti-Dark Solitons in a Single-Mode Fiber Laser," *Physics Letters A*, vol. 395, 2021. [CrossRef] [Google Scholar] [Publisher Link]
[4] Attila Fülöp et al., "High-Order Coherent Communications using Mode-Locked Dark-Pulse Kerr Combs from Microresonators," *Nature Communications*, vol. 9, pp. 1-8, 2018. [CrossRef] [Google Scholar] [Publisher Link]
[5] Mohammed S. Alshaykh et al., "Kerr Combs for Stimulated Brillouin Scattering Mitigation in Long-Haul Analog Optical Links," *Journal of Lightwave Technology*, vol. 37, no. 23, pp. 5773-5779, 2019. [Google Scholar] [Publisher Link]
[6] Jason D. McKinney, Vincent J. Urick, and John Briguglio, "Optical Comb Sources for High Dynamic-Range Single-Span Long-Haul Analog Optical Links," *IEEE Transactions on Microwave Theory and Techniques*, vol. 59, no. 12, pp. 3249-3257, 2011. [CrossRef] [Google Scholar] [Publisher Link]
[7] Yuri S. Kivshar, and Barry Luther-Davies, "Dark Optical Solitons: Physics and Applications," *Physics Reports*, vol. 298, no. 2-3, pp. 81-197, 1998. [CrossRef] [Google Scholar] [Publisher Link]
[8] Yaoyao Qi et al., "Generation of Bright–Dark Pulse Pairs in the Er-Doped Mode-Locked Fiber Laser based on Doped Fiber Saturable Absorber," *Photonics*, vol. 11, no. 6, pp. 1-10, 2024. [CrossRef] [Google Scholar] [Publisher Link]
[9] Yapeng Xie et al., "Machine Learning Applications for Short-Reach Optical Communication," *Photonics*, vol. 9, no. 1, pp. 1-38, 2022. [CrossRef] [Google Scholar] [Publisher Link]
[10] Yvan Pointurier, "Machine Learning Techniques for Quality of Transmission Estimation in Optical Networks," *Journal of Optical Communications and Networking*, vol. 13, no. 4, pp. 60-71, 2021. [CrossRef] [Google Scholar] [Publisher Link]
[11] Haci Mehmet Baskonus, Tukur Abdulkadir Sulaiman, and Hasan Bulut, "Bright, Dark Optical and Other Solitons to the Generalized Higher-Order NLSE in Optical Fibers," *Optical and Quantum Electronics*, vol. 50, 2018. [CrossRef] [Google Scholar] [Publisher Link]
[12] Houria Trik et al., "Dark Solitons in an Extended Nonlinear Schrödinger Equation with Higher-Order Odd and Even Terms," *Optik*, vol. 164, pp. 661-670, 2018. [CrossRef] [Google Scholar] [Publisher Link]
[13] Saroja V. Siddamal, R.M. Banakar, and B.C. Jinaga, "Split-Step Method in the Analysis and Modeling of Optical Fiber Communication System," *Advances in Computing, Communication and Control*, pp. 254-261, 2011. [CrossRef] [Google Scholar] [Publisher Link]
[14] Hang Yang et al., "Fast and Accurate Waveform Modeling of Long-Haul Multichannel Optical Fiber Transmission using a Hybrid Model-Data Driven Scheme," *Journal of Lightwave Technology*, vol. 40, no. 14, pp. 4571-4580, 2022. [CrossRef] [Google Scholar] [Publisher Link]
[15] Ezra Ip et al., "DAS Over 1,007-km Hybrid Link With 10-Tb/s DP-16QAM Co-Propagation Using Frequency-Diverse Chirped Pulses," *Journal of Lightwave Technology*, vol. 41, no. 4, pp. 1077-1086, 2023. [CrossRef] [Google Scholar] [Publisher Link]
[16] Stavros Deligiannidis et al., "Multichannel Nonlinear Equalization in Coherent WDM Systems based on Bi-Directional Recurrent Neural Networks," *Journal of Lightwave Technology*, vol. 42, no. 2, pp. 541-549, 2024. [CrossRef] [Google Scholar] [Publisher Link]
[17] Kyo Inoue, and Koji Igarashi, "Nonlinear Wave Equation for Wavelength/Polarization Multiplexed Signals in Fiber Transmission," *Optics Continuum*, vol. 2, no. 69, pp. 1331-1339, 2023. [CrossRef] [Google Scholar] [Publisher Link]
[18] Aly R. Seadawy, and Nadia Cheemaa, "Propagation of Nonlinear Complex Waves for the Coupled Nonlinear Schrödinger Equations," *Physica A: Statistical Mechanics and its Applications*, vol. 529, 2019. [CrossRef] [Google Scholar] [Publisher Link]
[19] Mamta Kapoor, "Dark Soliton Solutions of Cubic-Quartic Nonlinear Schrödinger Equation via Sumudu HPM," *Results in Optics*, vol. 21, pp. 1-15, 2025. [CrossRef] [Google Scholar] [Publisher Link]
[20] Paramjit Kaur, Divya Dhawan, and Neena Gupta, "Mitigation of Nonlinearities in Long-Haul DWDM Soliton-Based Communication System," *Journal of Optical Communications*, vol. 45, no. S1, pp. 1031-1038, 2023. [CrossRef] [Google Scholar] [Publisher Link]
[21] Kovendhan Vijayan et al., "Phase-Sensitively Amplified Wavelength-Division Multiplexed Optical Transmission Systems," *Optics Express*, vol. 29, no. 21, pp. 33086-33096, 2021. [CrossRef] [Google Scholar] [Publisher Link]
[22] Muhammad Amin S. Murad et al., "The Fractional Soliton Solutions and Dynamical Investigation for Planar Hamiltonian System of Fokas Model in Optical Fiber," *Alexandria Engineering Journal*, vol. 121, pp. 27-37, 2025. [CrossRef] [Google Scholar] [Publisher Link]
[23] Kang-Jia Wang et al., "The Perturbed Chen–Lee–Liu Equation: Diverse Optical Soliton Solutions and Other Wave Solutions," *Advances in Mathematical Physics*, vol. 2024, no. 1, pp. 1-13, 2024. [CrossRef] [Google Scholar] [Publisher Link]
[24] Asbah Masih, and Gurjit Kaur, "Machine Learning-Based Regression Models for Predicting Signal Quality of Dense Wavelength Division Multiplexing Optical Communication Network," *International Journal of Communication Systems*, vol. 36, no. 13, 2023. [CrossRef] [Google Scholar] [Publisher Link]
[25] Guanju Peng et al., "Coherent All-Optical Reservoir Computing for Nonlinear Equalization in Long-Haul Optical Fiber Communication Systems," *Optics and Laser Technology*, vol. 174, 2024. [CrossRef] [Google Scholar] [Publisher Link]
[26] Wafy M. Hasan et al., "Exploring Highly Dispersive Optical Solitons and Modulation Instability in Nonlinear Schrödinger Equations," *Scientific Reports*, vol. 15, pp. 1-20, 2025. [CrossRef] [Google Scholar] [Publisher Link]

[27] Mohammed F. Shehab et al., "Analytic Solutions for Stochastic Fourth-Order (2+1)-Dimensional NLSE with Higher-Order Terms," *Optical and Quantum Electronics*, vol. 56, 2024. [CrossRef] [Google Scholar] [Publisher Link]
[28] Annamalai Muniyappan et al., "Exploring the Dynamics of Dark and Singular Solitons in Optical Fibers using Extended Rational Sinh–Cosh and Sine–Cosine Methods," *Symmetry*, vol. 16, no. 5, pp. 1-20, 2024. [CrossRef] [Google Scholar] [Publisher Link]
[29] A. Muniyappan et al., "Chirped Dark Soliton Propagation in Optical Fiber under a Self Phase Modulation and a Self-Steepening Effect for Higher Order Nonlinear Schrödinger Equation," *Optical and Quantum Electronics*, vol. 56, 2024. [CrossRef] [Google Scholar] [Publisher Link]
[30] Song Yang et al., "Recent Advances and Challenges on Dark Solitons in Fiber Lasers," *Optics and Laser Technology*, vol. 152, 2022. [CrossRef] [Google Scholar] [Publisher Link]
[31] Eugene Aban Chenui, and Alain Moïse Dikandé, "Soliton-Mode Proliferation Induced by Cross-Phase Modulation of Harmonic Waves by a Dark-Soliton Crystal in Optical Media," *Microwave and Optical Technology Letters*, vol. 63, no. 10, pp. 2681-2688, 2021. [CrossRef] [Google Scholar] [Publisher Link]
[32] N. Nasreen et al., "Propagation of Optical Pulses in Fiber Optics Modeled by Coupled Space-Time Fractional Dynamical System," *Alexandria Engineering Journal*, vol. 73, pp. 173-187, 2023. [CrossRef] [Google Scholar] [Publisher Link]
[33] Faissal Mansouri et al., "Chirped Localized Pulses in a Highly Nonlinear Optical Fiber with Quintic Non-Kerr Nonlinearities," *Results in Physics*, vol. 43, 2022. [CrossRef] [Google Scholar] [Publisher Link]
[34] Xinyu Liu et al., "Bi-Directional Gated Recurrent Unit Neural Network-Based Nonlinear Equalizer for Coherent Optical Communications," *Optics Express*, vol. 29, no. 4, pp. 5923-5938, 2021. [CrossRef] [Google Scholar] [Publisher Link]
[35] Weijie Sheng et al., "Complex-Valued Recurrent Neural Network Equalizer with Low Complexity for a 120-Gbps 50-km Optical PAM-4 IM/DD System," *Optics Express*, vol. 32, no. 16, pp. 27624-27634, 2024. [CrossRef] [Google Scholar] [Publisher Link]
[36] Riyaz Saiyyed et al., "Comprehensive Analysis of Nonlinear Effects in Fiber Optic Communication Systems: Exploring SPM, XPM, SS, and FWM," *Journal of Optics*, 2025. [CrossRef] [Google Scholar] [Publisher Link]
[37] Li Wang et al., "PMD Estimation and its Enabled Feedforward Adaptive Equalization based on Superimposed FrFT Training Sequences," *Optics Letters*, vol. 46, no. 7, pp. 1526-1529, 2021. [CrossRef] [Google Scholar] [Publisher Link]
[38] Alper Demir, "Nonlinear Phase Noise in Optical-Fiber Communication Systems," *Journal of Lightwave Technology*, vol. 25, no. 8, pp. 2002-2032, 2007. [Google Scholar] [Publisher Link]
[39] Luís C.B. Silva et al., "Long-Haul Propagation Analysis of Dark Pulses Employing an Optical Recirculating Fiber Loop Technique," *Optics Communications*, vol. 495, 2021. [CrossRef] [Google Scholar] [Publisher Link]
[40] Gerd Keiser, *Fiber Optic Communication Networks*, Fiber Optic Communications, pp. 507-575, 2021. [CrossRef] [Google Scholar] [Publisher Link]
[41] Neveen G. A. Farag et al., "Extended Split-Step Fourier Transform Approach for Accurate Characterization of Soliton Propagation in a Lossy Optical Fiber," *Journal of Function Spaces*, vol. 2022, no. 1, pp. 1-17, 2022. [CrossRef] [Google Scholar] [Publisher Link]
[42] Emad H.M. Zahran et al., "Dark-Soliton Behaviors Arising from a Coupled Nonlinear Schrödinger System," *Results in Physics*, vol. 36, pp. 1-16, 2022. [CrossRef] [Google Scholar] [Publisher Link]
[43] Rui Jiang et al., "Data-Driven Method for Nonlinear Optical Fiber Channel Modeling based on Deep Neural Network," *IEEE Photonics Journal*, vol. 14, no. 4, pp. 1-8, 2022. [CrossRef] [Google Scholar] [Publisher Link]
[44] Xiaotian Jiang et al., "Physics-Informed Neural Network for Nonlinear Dynamics in Fiber Optics," *Laser & Photonics Reviews*, vol. 16, no. 9, 2022. [CrossRef] [Google Scholar] [Publisher Link]
[45] Wenting Wang et al., "Free-Space Terabit/s Coherent Optical Links via Platicon Frequency Microcombs," *eLight*, vol. 5, pp. 1-16, 2025. [CrossRef] [Google Scholar] [Publisher Link]